OBSERVATIONS OF RELATIVE HUMIDITY CONDITIONS REQUIRED FOR CIRRUS FORMATION

Andrew J. Heymsfield and Larry M. Miloshevich

National Center for Atmospheric Research,*
Boulder, Colorado

1. INTRODUCTION

The ice nucleation process at low temperatures plays a major role in the formation and evolution of cirrus clouds. Heymsfield and Miloshevich (1993, hereafter HM) used aircraft measurements in lenticular orographic wave clouds near Boulder, Colorado in 1989 (the Wave89 experiment), and a Lagrangian parcel model based on prescribed dynamics and detailed microphysics (HM; Heymsfield and Sabin 1989) to study the ice nucleation process over the temperature range -31 to -41°C. We will extend the conclusions of HM to colder temperatures, and investigate the RH and temperature requirements for ice nucleation using aircraft measurements from a similar orographic wave cloud experiment in 1990 (Wave90). We will then investigate the conditions required for ice nucleation in cirrus using aircraft measurements from FIRE II (the First ISCCP Research Experiment, Phase II) conducted near Coffeyville, Kansas in 1991.

2. THE WAVE90 EXPERIMENT

2.1 Instrument and experiment descriptions

During Wave90 the NCAR Sabreliner conducted upwind-downwind cloud penetrations in cold orographic wave clouds during five research flights in November 1990, along the Front Range of the Rocky Mountains in northern Colorado and Southern Wyoming. Successive constant-altitude cloud penetrations spanned the temperature range -32 to -56°C. From the 66 cloud penetrations conducted, we use in this analysis only those 31 penetrations which unambiguously penetrated the upwind edge of the cloud and whose paths were within 30 degrees of the wind direction. Only penetrations where ice nucle-

* The National Center for Atmospheric Research is sponsored by the National Science Foundation.

Corresponding author address: A. J. Heymsfield, NCAR, P.O. Box 3000, Boulder, CO 80307-3000.

ation is observed in the updraft are presented in this section; if the first detection of ice is in the downdraft, then ice nucleation occurred somewhere above the penetration level.

The aircraft instruments used in this study are the same as those described in HM, with one important exception. Particle sizes were measured in 31 size channels between 0.4 and 21 μm with the Particle Measuring Systems (PMS) FSSP-300. RH measurements were made with the NCAR airborne cryogenic hygrometer. Its accuracy was estimated to be $\pm$5% under the worst-case conditions of rapidly changing RH, and $\pm$2-3% when the RH changes slowly. The hygrometer's time response is qualitatively evaluated by comparison to fast-response (20 Hz) water vapor density measurements from a Lyman-alpha (L_α) probe. LWC measurements were made with a Rosemount icing probe (RICE) which has a detection threshold of 0.002 g m^{-3} (Heymsfield and Miloshevich 1989).

2.2 Aircraft measurements

Three constant-altitude wave cloud penetrations on two of the Wave90 research days represent the clouds and conditions encountered in the temperature range -35 to -56°C. The measurements illustrate characteristics of the ice nucleation process, particularly temperature dependences of the RH and droplet size upon freezing. All measurements are plotted vs. horizontal distance downwind. The cases are presented in order of decreasing temperature.

Fig. 1A, with minimum temperature -35°C, illustrates the smoothness of the updraft in these wave clouds. Droplets begin to grow in the updraft to sizes above 0.4 μm at distance coordinate x=7.5 km (Fig. 1C), when the RH is about 50%, well below ice-saturation (Fig. 1B). Droplet growth becomes rapid near water-saturation (Fig. 1D, x=9.5 km), with activated droplet concentrations (>3 μm) of 180 cm^{-3} arising from total concentrations (>0.4 μm) of 400 cm^{-3} (Fig. 1C). Ice nucleation occurs rapidly at x=13 km, as indicated by the simultaneous disappearance of LW detected by the RICE (horizontal bars), decrease in the FSSP-300 concentrations, and decrease in the RH to ice-saturation with a resulting increase in the mean size of (ice) particles larger than 3 μm. The air is then maintained at ice-saturation until all ice has sublimated (Fig. 1B, x=19 km). The RH and the L_α voltage show an excellent qualitative correlation, subject to a time delay in the RH measurements of about 4 s. [Note: all references to RH in this paper will be given with respect to water, including the RH corresponding to ice-saturation.]

Corresponding one-second FSSP-300 normalized size spectra (Fig. 2) first shows the growth of increasing concentrations of unactivated solution droplets above the 0.4 μm detection threshold (x=8.2-10.0 km), then, as the RH increases in the updraft, increasing concentrations of activated droplets (x=10.6 km, when the LWC has become great enough for detection by the RICE). Ice nucleation is signaled (x=12.9-13.5 km) by low concentrations of large particles as the RH decreases below 100%. The remaining unfrozen droplets

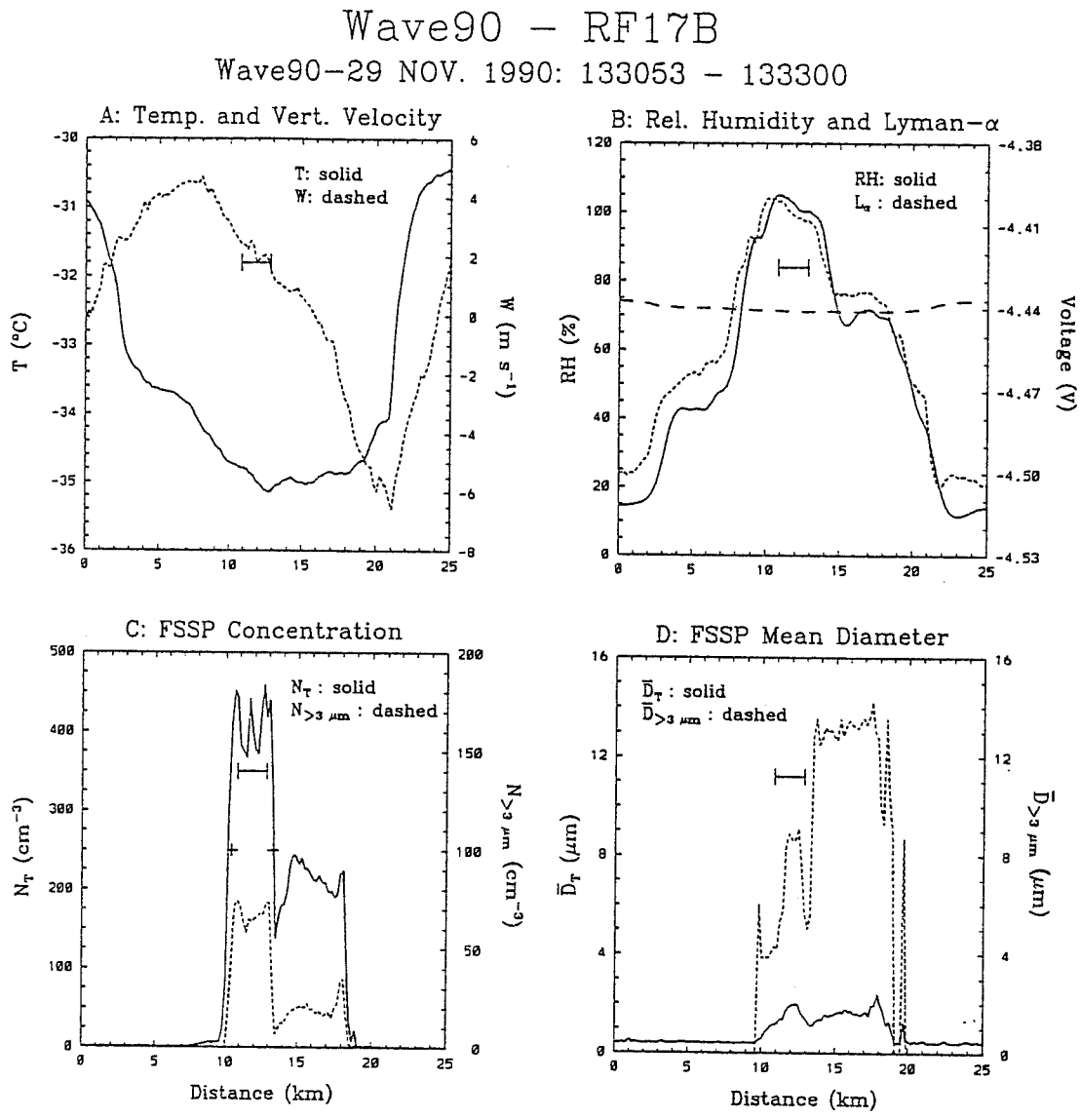

Figure 1: Sabreliner measurements from 29 Nov. 1990, 1330:53-1333:00 UTC. Horizontal axis is distance downwind from some initial point. (A) Temperature (T) and vertical velocity (W). (B) Relative humidity (RH) from the cryogenic hygrometer, and output voltage (V) from the Lyman-alpha (L_α) probe. An ice-saturation curve is shown (long dashes). (C) Particle concentrations from the FSSP-300: total concentration in the size range 0.4-21 μm (N_T), and concentration in the size range 2.73-21 μm ($N_{>3\mu m}$). (D) Mean diameters from the FSSP-300: for all size channels in the range 0.4-21 μm ($\overline{D}_T$), and for only size channels in the range 2.73-21 μm ($\overline{D}_{>3\mu m}$). Horizontal bars in all panels show where LW was detected by the RICE, above its 0.002 g m^{-3} detection threshold.

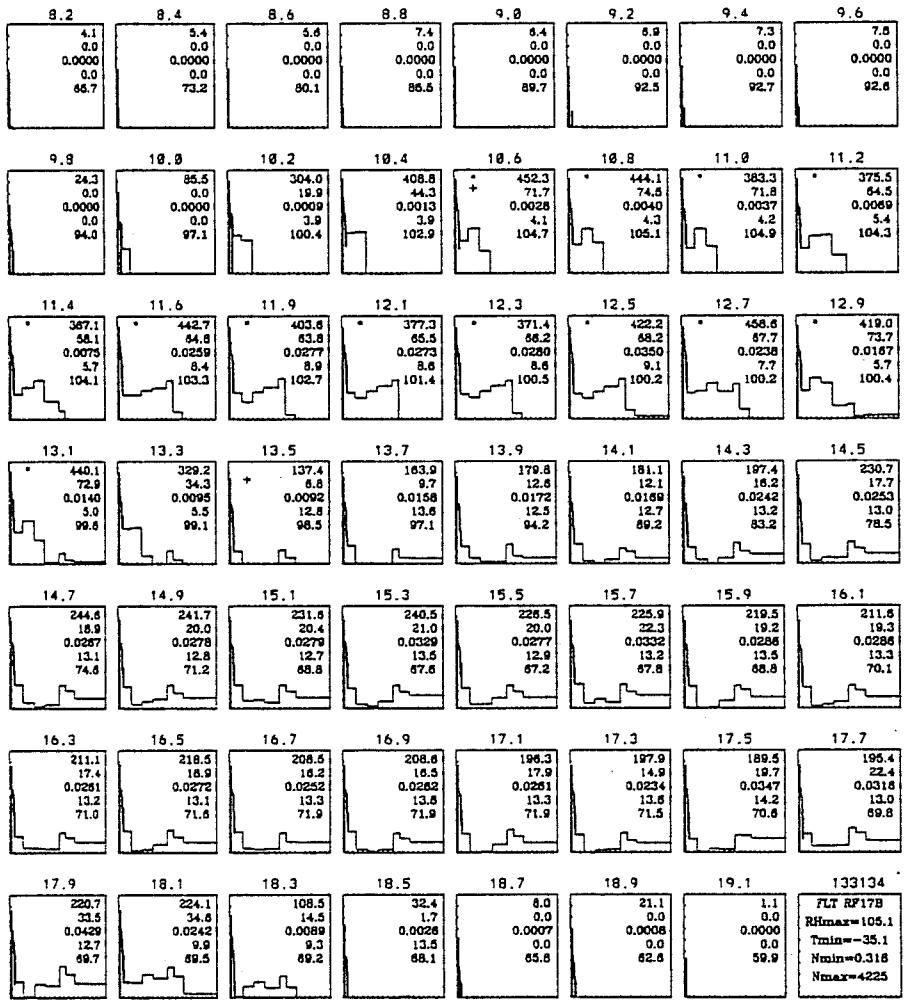

Figure 2: One-second FSSP-300 size spectra from 29 Nov. 1990. Distance coordinates above each plot (km) correspond to Fig. 1. Numbers within each plot, from top to bottom, are: total concentration (cm^{-3}) in the size range 0.4-21 μm; concentration in the size range 2.73-21 μm; "liquid" water content (g m^{-3}), assuming spheres with density 1 g cm^{-3}; mean diameter (μm) for all size channels in the range 2.73-21 μm; and RH from the cryogenic hygrometer (%). Asterisks indicate that LW was detected by the RICE. Logarithmic ordinates are normalized concentrations (cm^{-3} μm^{-1}), with minimum value -0.5 (0.316 cm^{-3} μm^{-1}), and increments of 0.5. Linear abscissa increments are each 1 μm.

evaporate, and the RICE signal disappears (even though the *implied* water content remains well above its detection threshold). [This water content calculation assumes all FSSP-300 particles are droplets, thus calculation of a water content >0.002 g m^{-3} when the RICE detects no LW suggests that the particles are ice.] The water content increases in the ice-supersaturated environment (x=13.5 to 15.3 km) until ice-saturation is reached and maintained. Finally, the ice sublimates, the air dries, and the submicron solution droplets disappear (x=17.9-19.1 km).

The penetration data at -37°C (Fig. 3) show signatures characteristic of ice nucleation at x=8.9 km, particularly the simultaneous decrease in RH, as indicated qualitatively by the L_α voltage (the hygrometer was inoperative on this portion of the flight), and the sharp decrease in *total* concentration coincident with the appearance of particles larger than 3 μm. Unlike Fig. 1D, where activated droplets grew large before freezing, ice nucleation at -37°C occurs when maximum droplet sizes are between 0.4 and 3 μm, and the LWC was never high enough for detection by the RICE. This observation validates the modeling prediction given by HM that the characteristic FSSP-100 and RICE signatures of homogeneous ice nucleation could not be seen below -36°C as a result of instrument detection thresholds.

The associated FSSP-300 size spectra (Fig. 4) show the growth of droplets to a maximum size of 5-7 μm (x= 8.9 km), followed immediately by spectral broadening due to ice nucleation and rapid ice growth (x=8.9-9.3 km). Note that high concentrations of submicron solution droplets coexist with the ice, even when the RH has presumably dropped to ice-saturation.

Below -56°C (Fig. 5) the RH and FSSP signatures suggest homogeneous freezing (x= 10.5 km), when the peak RH is 73%. The RH remains within 4% of ice-saturation until all ice has sublimated (x=20.7 km), after which the RH decreases rapidly.

2.3 Discussion and implications of the Wave90 measurements

Those penetrations where ice nucleation was directly observed in the updraft define the temperature-dependence of the RH required for ice nucleation in the wave clouds (Fig. 7, large circles). The observed peak RH decreases monotonically from water-saturation at -39°C to 73% at -56°C, and defines an envelope (Fig. 7, solid curve) given in Eq. 1 (where T is in °C).

$$RH_{hn} = 188.92 + 2.81T + 0.013336T^2 \quad (1)$$

The Sassen and Dodd (1989) freezing point depression curve, calculated assuming ammonium sulfate CCN, appears in Fig. 7. Above -40°C, both theory and observation suggest that conditions near water-saturation are required for ice nucleation, but below -40°C the observed temperature-dependence is steeper than that expected from ammonium sul-

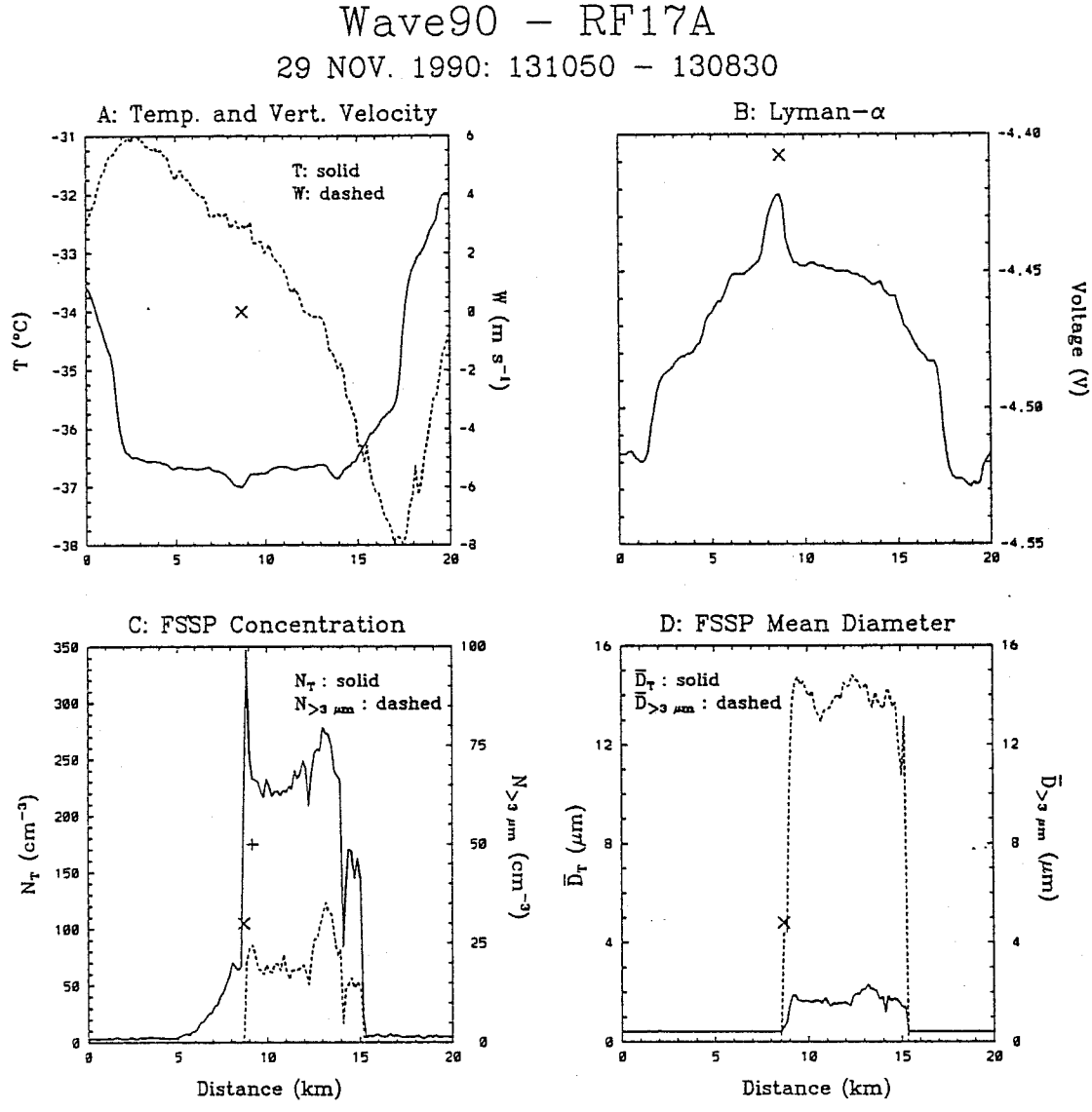

Figure 3: Same as Fig. 1, except for 1310:50-1308:30 UTC. No cryogenic hygrometer data is available.

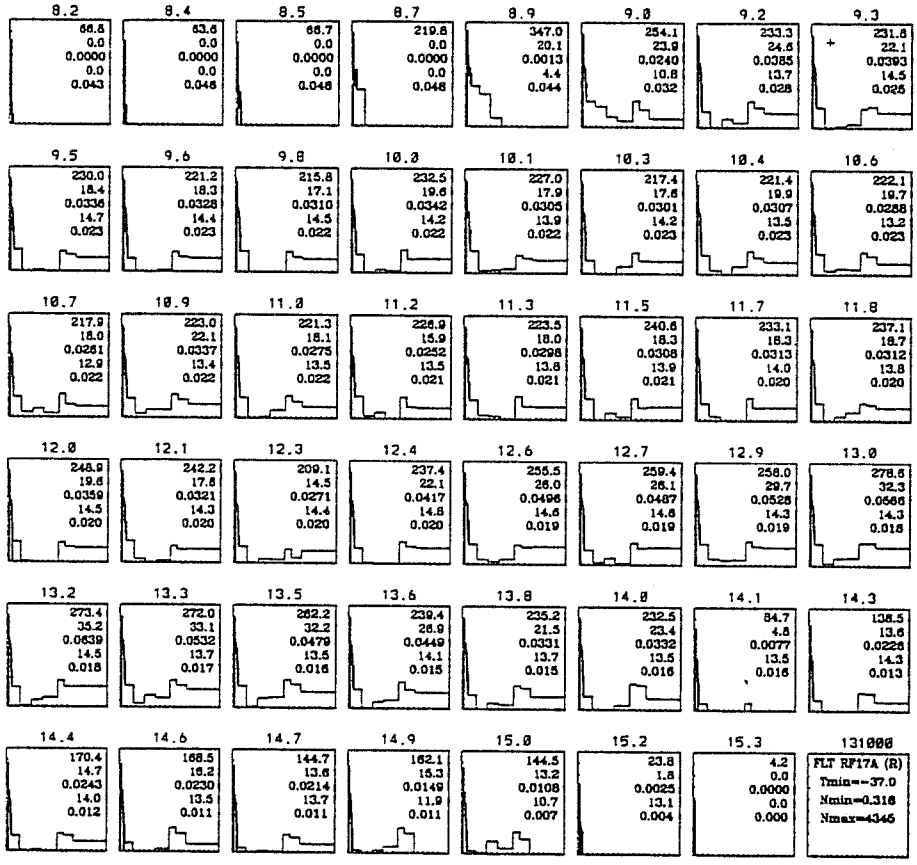

Figure 4: One-second FSSP-300 size spectra from 29 Nov. 1990, corresponding to Fig. 3. All scales and numbers have the same meaning as in Fig. 2, except the L_α voltage is given in place of the RH (relative to the minimum value during this time period).

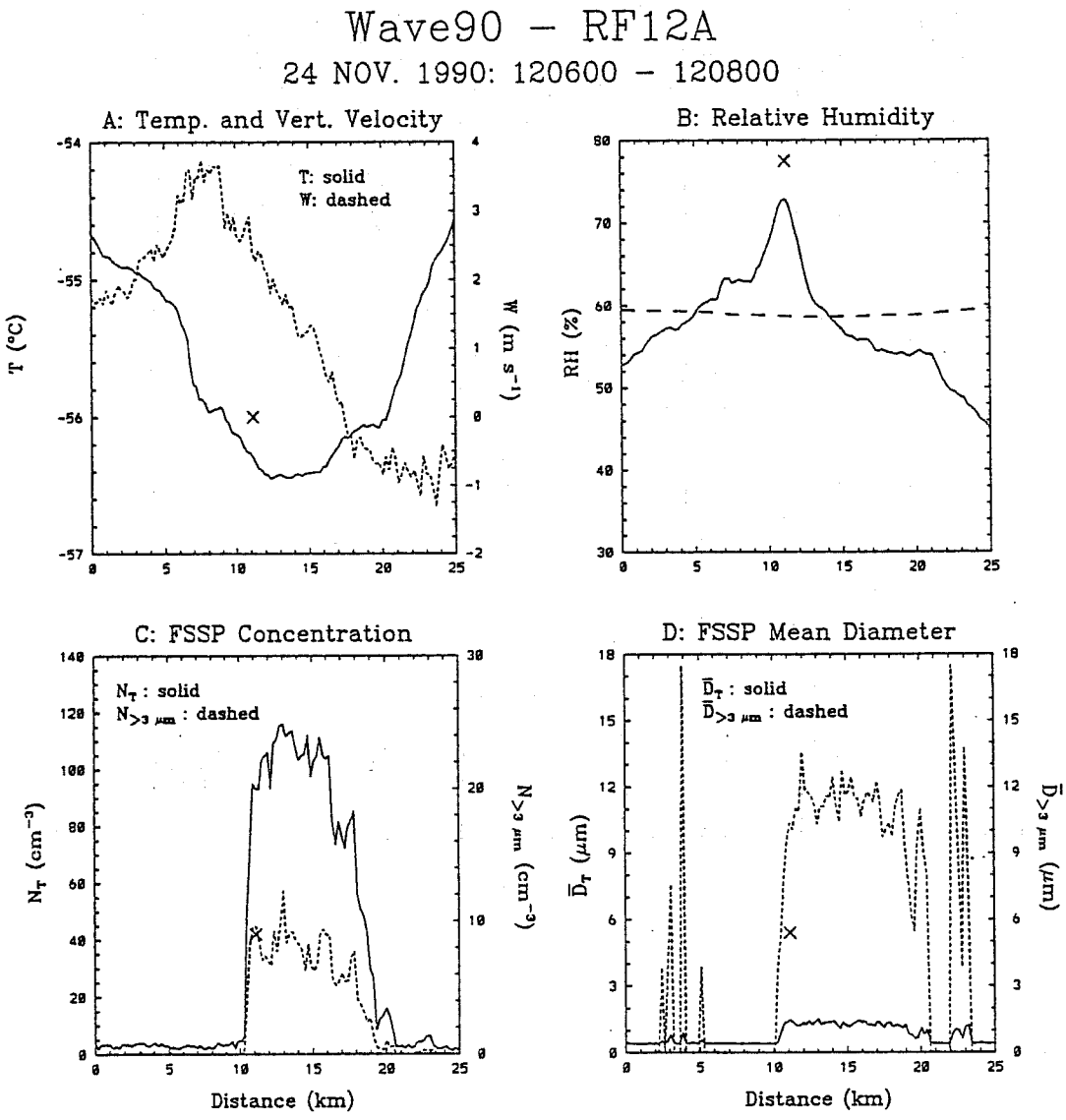

Figure 5: Sabreliner measurements from 24 Nov. 1990, 1206:00-1208:00 UTC. All curves and symbols are the same as in Fig. 1, except the Lyman-alpha measurements are not plotted. A reference 'X' marks the location of the peak RH value.

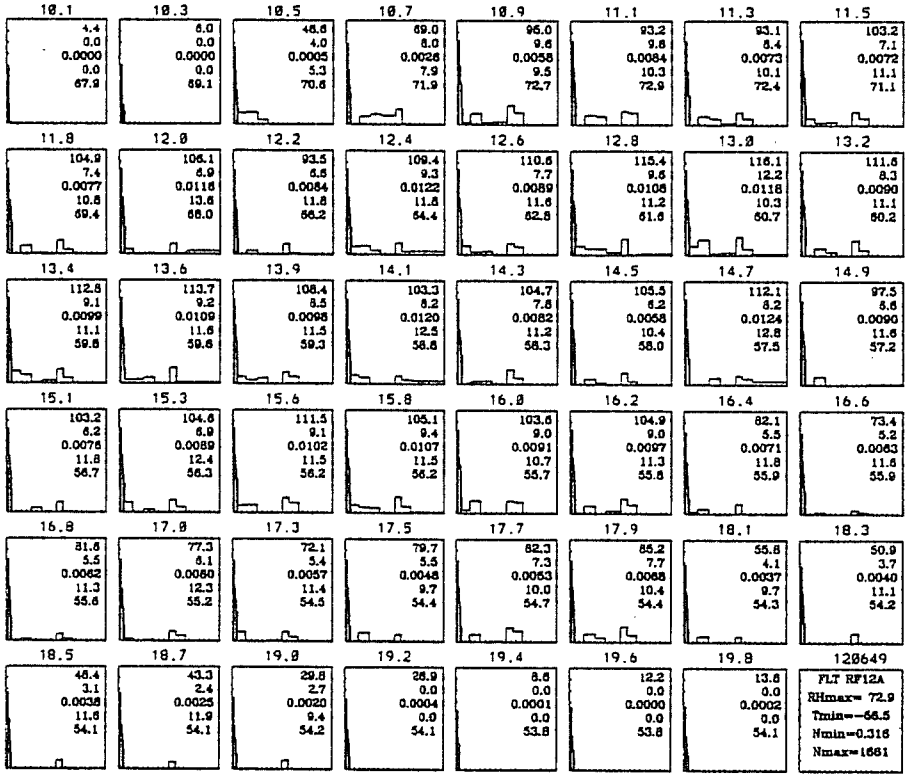

Figure 6: One-second FSSP-300 size spectra from 24 Nov. 1990, corresponding to Fig. 5. All scales and numbers have the same meaning as in Fig. 2.

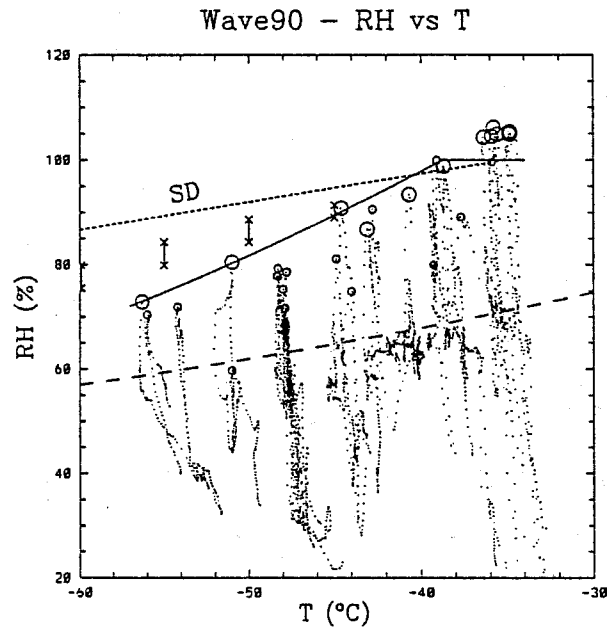

Figure 7: RH as a function of temperature for 34 cloud penetrations from five Wave90 research flights. Circles mark the peak RH for each penetration, either when the peak was detected in the updraft (large circles), or in the downdraft (small circles). Curves shown are the SD freezing point depression curve (short dashes), the ice-saturation curve (long dashes), and the RH_{hn} curve described in the text (solid). Each pair of 'x' symbols shows the range in RH at which sulfuric acid solution droplets of initial sizes D_o=0.1 and 1.0 μm freeze homogeneously, as described in the text.

fate CCN. Below about -50°C, ice nucleation is observed below even the deliquescence RH of ammonium sulfate (about 80%), suggesting the possibility of a different CCN chemical composition. We modeled the freezing of sulfuric acid solution droplets by homogeneous ice nucleation and have concluded that the observations are consistent with the homogeneous freezing of sulfuric acid solution droplets (Fig. 7).

3. THE FIRE II-CIRRUS EXPERIMENT

3.1 Instrument and experiment descriptions

The NCAR King Air and Sabreliner participated in FIRE II, an intensive study of cirrus cloud systems involving aircraft, ground-based remote sensors, balloon-borne in situ sensors, and satellite measurements. In this study we consider only measurements from the King Air because it concentrated on in-cloud measurements, had an FSSP-100 onboard, and flies slower, introducing fewer degrading effects on data quality. Furthermore, we consider only measurements from the first seven FIRE II research flights, due to subsequent failure of the cryogenic hygrometer.

The King Air had key instrumentation similar to that described for the Sabreliner during the Wave90 experiment. Droplets were measured with an FSSP-100, which classified droplet sizes in 15 channels between 3 and 45 μm, but this probe is only minimally useful in characterizing small particles when large and complex ice crystals are present. Ice crystal size distributions were measured with Particle Measuring Systems Inc. (PMS) two-dimensional (2D) imaging probes, above 50 μm for the 2D-C and 200 μm for the 2D-P. Lagrangian "vertical" profiles of cloud particle size distributions and ice crystal habits were measured with a balloon-borne formvar ice crystal replicator (Miloshevich et al. 1992), which ascended at 5 m s^{-1} and has a sample volume of approximately 5 L s^{-1}. The cryogenic hygrometer onboard the King Air had not previously been evaluated during a field experiment, although it was calibrated in the laboratory immediately prior to FIRE II.

3.2 FIRE II aircraft and replicator measurements

We present aircraft and replicator measurements in this subsection directed first at understanding the RH conditions required for initial cirrus cloud formation, then at understanding the parameters governing microphysical evolution and the potential for ongoing ice nucleation in cirrus.

3.2.1 RH conditions for ice initiation

Observations of ice-supersaturated regions devoid of ice crystals set a lower bound on the RH required for ice initiation, independent of any assumed ice nucleation mechanism. 12.5% of all RH measurements in clear air below -30°C during flights RF02 through RF07 were ice-supersaturated (Fig. 8), with peak ice-supersaturations of 20%. These observations suggest the possibility that either heterogeneous ice nucleation mechanisms (e.g. deposition or condensation-freezing modes) require higher ice-supersaturations to become

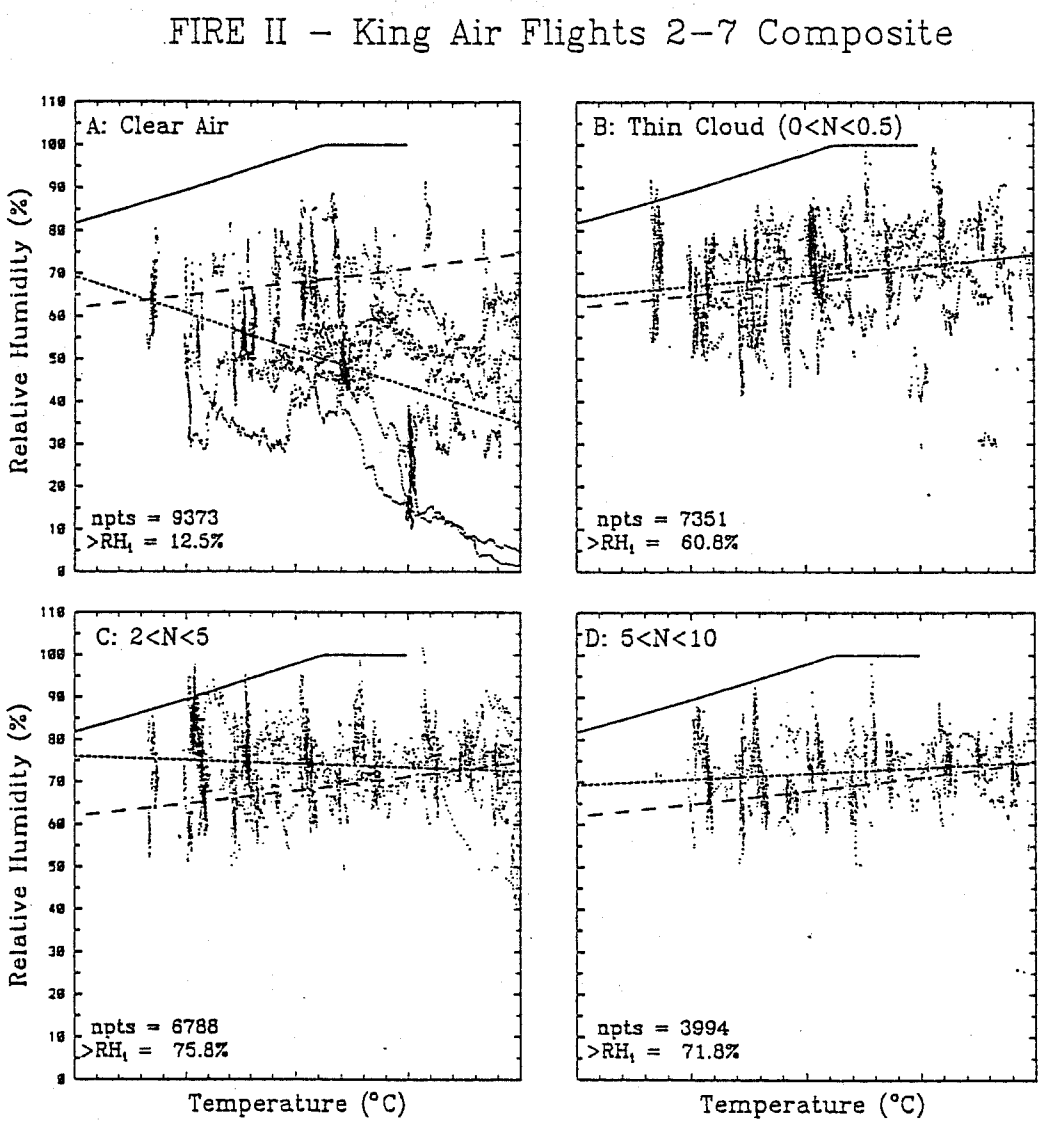

Figure 8: RH as a function of temperature for King Air flights RF02-RF07, 13 Nov. to 26 Nov. 1991. A: All times when no particles were detected in the 1 Hz 2D-C measurements. The ice-saturation curve (long dashes), RH_{hn} (solid), and RH_{hn}-10% (short dashes) are shown for reference, as is the percentage of the total number of points ("npts") which lie above the ice-saturation curve (">RH_i"); (B) Concentrations in the range $0<N<0.5\ L^{-1}$; (C) $2<N<5\ L^{-1}$; and (D) $5<N<10$. Curves show ice-saturation (long dashes), RH_{hn} (solid), and a least squares linear fit to the measurements (short dashes).

active, or there exists a dearth of active ice-forming nuclei in the upper troposphere. [The FSSP-100 measurements verified that these were truly clear air regions, at least for particle sizes down to 3 μm.]

3.2.2 Dependence of RH on ice concentration

The in-cloud RH for all instances below -30°C during King Air flights RF02 through RF07 is shown in Figs. 8B-D, given as a function of temperature and partitioned by ice crystal concentration. Although much more data of this type is required before making conclusive statements about water vapor distributions and ice nucleation processes in cirrus, the relatively small sample in Fig. 8 suggests that:

- Deviations from ice-saturation in cirrus are common and substantial, with peak ice-supersaturations exceeding 25%.
- Peak ice-supersaturation decreases with increasing ice concentration; the low vapor depletion rates resulting from low ice concentrations allow high ice-supersaturations to develop in updrafts, whereas the higher vapor depletion rates resulting from higher ice concentrations prevent such large ice-supersaturations from developing.
- Ice-supersaturations exceeding RH_{hn} suggest there is the potential to nucleate new ice crystals if the concentrations are low enough.

3.3 Vertical profiles of cirrus microphysics

We have analyzed replicator data from five FIRE II cases to understand the vertical structure and development of cirrus. Representative size spectra were derived for locations near cloud top, near cloud base, and throughout the cloud depth wherever distinct changes in microphysical properties were noted.

Inspection of the ice crystals revealed the presence of two microphysically distinct regions in all cases: a "sublimation zone" characterized the lower portion of each cloud, presumably formed when ice crystals fell into ice-subsaturated air, and an upper "growth zone" characterized by pristine ice crystals with sharp edges, in which the air is presumably ice-supersaturated. Aggregation of ice crystals was found to be common in the sublimation zones. Complex cloud layering was also encountered.

The ice crystal concentration generally decreases from near cloud top to cloud base, while the mean diameter increases from cloud top to near cloud base, then decreases at cloud base, presumably as the ice crystals sublimate. The size spectra broaden considerably from cloud top to cloud base, as reflected by both the standard deviation of the diameters and the maximum ice crystal diameter.

3.4 Discussion and implications of the FIRE II-Cirrus measurements

3.4.1 Conceptual model of cirrus formation and evolution

The replicator and aircraft measurements show that the observed cirrus clouds, and perhaps cirrus in general, are characterized by three microphysically distinct regions: highly

ice-supersaturated ice production regions, which are near cloud top in an existing cloud; ice-supersaturated growth regions; and sublimation regions near cloud base, which arise from fallout of ice crystals into ice-subsaturated air.

Both the formation and decay of ice production regions are controlled by the RH, which in turn is established by the balance between vapor depleted by existing ice concentrations and vapor supplied by the updraft. Ice production will occur in clear air whenever the RH exceeds the threshold value given approximately by RH_{hn}-10% (Eq. (1)); new in-cloud ice production may occur at cloud top in updrafts whenever ice concentrations are $\sim$10 L^{-1} and the RH exceeds a vertical velocity-dependent threshold bounded approximately by RH_{hn} and RH_{hn}-10%. The resulting ice concentration modulates the RH, which in turn modulates the ice production rate. Growth of ice crystals depletes the vapor, reduces the RH, and either slows or stops ice production. The updraft speed, and vapor depletion by ice at lower levels, affect the RH at cloud top and largely determine whether ice production will be rapid or slow. Rapid ice production results in high ice concentrations which reduce the RH sufficiently to halt further ice production; slow ice production results in low ice concentrations, which may result in slow, continuous ice production. Ice produced in generating regions is dispersed horizontally and falls into lower levels, broadening and thickening the cloud and establishing the three microphysically-distinct cloud regions mentioned above.

4. SUMMARY AND CONCLUSIONS

4.1 Wave90

Analysis of measurements in wave clouds over the temperature range -30 to -56°C with vertical velocities of several m s^{-1}, augmented by numerical modeling of homogeneous ice nucleation, led to the following observations and conclusions:

- The measurements are consistent with the growth of solution droplets and subsequent *homogeneous* ice nucleation, throughout the temperature range of the study, based partially on characteristic instrument signatures and modeling of homogeneous ice nucleation developed in HM.
- The maximum RH in the wave clouds (RH_{hn}, given by Eq. (1)) is controlled by homogeneous ice nucleation, and ranges from water-saturation at temperatures above -39°C to 73% at -56°C. RH_{hn} defines the RH required for cloud formation, for the updraft speeds and CCN properties encountered in the wave clouds.
- The temperature-dependence of Eq. (1) and numerical modeling suggest that the chemical composition of the active CCN in the wave clouds is more consistent with sulfuric acid than ammonium sulfate.

4.2 FIRE II-Cirrus

An analysis of relative humidity and temperature data led to the following observations and conclusions.

- Ice nucleation in clear air in the upper troposphere will occur whenever the RH exceeds a threshold value given approximately by RH_{hn}-10%.
- A negative feedback between ice concentration and ice-supersaturation allows the RH condition for new ice nucleation (approximately RH_{hn}) to develop only in cirrus regions where ice concentrations are low; furthermore, the most favorable location for new ice nucleation in cirrus is at cloud top, because fallout of existing ice crystals depletes the vapor at lower cloud levels.
- New ice nucleation in cirrus is a self-limiting process, since the ice production rate increases with increasing RH. If the ice production rate is rapid, the resulting high ice concentrations will deplete the vapor and new ice nucleation will cease; if the ice production rate is slower, the lower ice concentrations may decrease the RH only enough to result in slow, continuous ice production.
- The vertical structure of cirrus generally consists of three microphysically distinct regions: a highly ice-supersaturated ice production region near cloud top, an ice-supersaturated ice crystal growth region, and a sublimation region near cloud base formed by fallout of ice into ice-subsaturated air.
- The observations and numerical modeling were generalized in the form of a conceptual model of cirrus formation and evolution.

Acknowledgements

We gratefully acknowledge Drs. W. (Al) Cooper and Charles Knight (NCAR) for many helpful discussions. The support of the NCAR Research Aviation Facility was instrumental to this study, in particular the efforts of Paul Spyers-Duran, Alan Schanot, Jr, and Dave McFarland. This work was supported in part by NASA/FIRE (grant no. L-98100B).

REFERENCES

Heymsfield, A. J., and L. M. Miloshevich, 1989: Evaluation of liquid water measuring instruments in cold clouds sampled during FIRE. *J. Atmos. Oc. Tech.*, **6**, 378-388.

Heymsfield, A. J., and R. M. Sabin, 1989: Cirrus crystal nucleation by homogeneous freezing of solution droplets. *J. Atmos. Sci.*, **46**, 2252-2264.

Heymsfield, A. J., and L. M. Miloshevich, 1993: Homogeneous Ice Nucleation and Supercooled Liquid Water in Orographic Wave Clouds. *J. Atmos. Sci.*, **50**, 2335-2353.

Miloshevich, L. M., A. J. Heymsfield, and P. M. Norris, 1992: Microphysical measurements in cirrus clouds from ice crystal replicator sondes launched during FIRE-II. Proceedings of the 11th International Conference on Clouds and Precipitation, Montreal, Quebec, Canada, 17-21 August, 1992.

Sassen, K. and G. C. Dodd, 1989: Haze particle nucleation simulations in cirrus clouds, and applications for numerical modeling and lidar studies. *J. Atmos. Sci.*, **46**, 3005-3014.